Vortex-assisted mechanism of photon counting in a superconducting nanowire single-photon detector revealed by external magnetic field

D. Yu. Vodolazov,[1,2] Yu. P. Korneeva,[3] A. V. Semenov,[3,4] A. A. Korneev,[3,4,5] and G. N. Goltsman[3,5]
[1]*Institute for Physics of Microstructures, Russian Academy of Sciences, 603950 Nizhny Novgorod, GSP-105 Russia*
[2]*Lobachevsky State University of Nizhny Novgorod, 23 Gagarin Avenue, 603950 Nizhny Novgorod, Russia*
[3]*Moscow State Pedagogical University, 1 M. Pirogovskaya Street, 119991 Moscow, Russia*
[4]*Moscow Institute of Physics and Technology, 9 Institutsky Lane, 141700 Dolgoprudny, Moscow Region, Russia*
[5]*National Research University—Higher School of Economics, 20 Myasnitskaya Street, 101000 Moscow, Russia*
(Received 13 May 2015; revised manuscript received 29 June 2015; published 4 September 2015)

We use an external magnetic field to probe the detection mechanism of a superconducting nanowire single-photon detector. We argue that the hot belt model (which assumes partial suppression of the superconducting order parameter Δ across the whole width of the superconducting nanowire after absorption of the photon) does not explain observed weak-field dependence of the photon count rate (PCR) for photons with $\lambda = 450$ nm and noticeable *decrease* of PCR (with increasing the magnetic field) in a range of the currents for photons with wavelengths $\lambda = 450$–1200 nm. Found experimental results for all studied wavelengths can be explained by the vortex hot spot model (which assumes partial suppression of Δ in the area with size smaller than the width of the nanowire) if one takes into account nucleation and entrance of the vortices to the photon induced hot spot and their pinning by the hot spot with relatively large size and strongly suppressed Δ.

DOI: 10.1103/PhysRevB.92.104503 PACS number(s): 74.25.N−, 74.25.F−, 85.25.Pb

I. INTRODUCTION

The main idea of a superconducting nanowire single-photon detector (SNSPD) is based on destruction of the superconductivity by the absorbed high-energy photon (which produces hot quasiparticles) in a relatively large area of the superconducting nanowire [1]. The appearance of such a region decreases the superconducting properties of the nanowire and leads to the resistive state (if transport current I exceeds some critical value) which is visible via appearance of the voltage. The first realization of such a detector was done in 2001 [2] and since that time there have been many theoretical [3–9] and experimental works (for review see [10]) which aimed to understand the physical details of its working mechanism and to improve its characteristics.

Despite a clear main idea why SNSPD works there are still debates about details of the appearance of the resistive state in SNSPD. These debates are connected with the absence of rigorous study (which needs the solution of kinetic equations coupled with the equation for the superconducting order parameter) of the initial stage of the response of the superconducting nanowire on the absorbed photon. In the set of theoretical works [1,3,7,8] referenced here authors used approaches which are similar to the Rothwarf-Taylor model [11], and their quantitative validity is questionable in the case when there is a spatial gradient of superconducting order parameter Δ. Nevertheless in the literature one may find two ideas about what happens after photon absorption: the photon creates a hot spot (HS) or hot belt. According to the hot spot model the absorbed photon creates a region with locally suppressed superconductivity (partially or completely) with the size smaller than the width of the nanowire [3–5,7–9]. As a result the superconducting current has to crowd near the hot spot and in [5,8,9] it is argued that the superconducting state becomes unstable at the detection current I_{det} (which is smaller than the critical current of the nanowire without the hot spot) due to nucleation and motion of the vortices.

Authors of the hot belt model [6] assume that the absorbed photon creates hot quasiparticles which are uniformly distributed across the whole width of the nanowire and it results in the appearance of some kind of weak link. The critical current I_c^{belt} of the nanowire with the hot belt (weak link) is smaller than the critical current of the nanowire I_c and when $I_c^{belt} < I < I_c$ the resistive state is realized after absorption of the photon. Vortices are involved in the hot belt model in order to explain smooth dependence of the detection efficiency (DE) of SNSPD on the applied current—the finite DE at $I < I_c^{belt}$ in this model is connected with the thermoactivated vortex entrance via the edge of the nanowire and its motion heats the nanowire and provides large voltage response. Note that in the hot spot model considered in [9] the smooth dependence DE(I) appears also from dependence of I_{det} on the transverse coordinate x of the hot spot in the nanowire.

From here on we will use the definition "intrinsic detection efficiency" (IDE) to indicate the probability to have resistive response in the superconducting nanowire after photon absorption (IDE = 1 means that each absorbed photon produces resistive response). Detection efficiency in real detectors is always smaller than IDE because absorption in the detector is less than unity. With this definition IDE is the intrinsic characteristic of the superconducting nanowire and not the whole detection system. Experimental dependence IDE(I) could be found if the photon count rate (PCR) saturates at large currents and IDE(I)= PCR(I)/PCR$_{sat}$.

To distinguish experimentally which of these two models is more relevant to the detection mechanism of SNSPD one may use the external magnetic field. The hot belt model predicts the parallel shift of dependence PCR(I) [or IDE(I)] in the direction of small currents with increasing magnetic field. This result directly comes from decay of I_c^{belt} in the magnetic field—a well-known result following from the theory of Josephson junctions [12] and narrow superconducting films [13]. The hot spot model of [9] predicts more complicated behavior,

with a noticeable shift of IDE(I) at low currents (where IDE $\lesssim 0.1$ is due to the thermoactivated vortex entrance to the hot spot—like in the hot belt model) and much weaker-field dependence at the currents where IDE $\gtrsim 0.1$ and vortices appear in the nanowire without any fluctuations. Moreover this model predicts *decrease* of PCR at the currents, where PCR saturates.

A recent experiment on a MoSi based SNSPD [14] discards the hot belt model for this detector. It was found that for a high-energy photon ($\lambda = 450$ nm) detection efficiency practically did not vary in the wide range of the magnetic fields at both the currents where IDE $\ll 1$ and IDE ~ 1. This result also discards the possibility of photon detection via thermoactivated vortex entry in the hot spot model of [9]. For photons with larger wavelength ($\lambda = 600$–1000 nm) dependence DE(I) shifted in the direction of smaller currents with increase of the magnetic field. The found result—the larger λ, the larger the shift—is also in contrast with prediction of the hot belt model where one could expect larger dependence on magnetic field for photons with smaller λ (in this case Δ should be suppressed more strongly in the hot belt region and one needs a smaller magnetic field to suppress $I_c^{\rm belt}$). In [9] no calculations were made for field-dependent IDE for photons with different energies.

In the present work we study the effect of the magnetic field on dependence PCR(I) of the SNSPD based on NbN. Qualitatively for all studied NbN detectors we find the same results as for the MoSi based SNSPD. Also we find an effect which was not observed for the MoSi SNSPD and which was theoretically predicted in [9]—external magnetic field decreases PCR (in a range of currents) and shifts the current, where PCR saturates, to larger values. To explain different field dependences of PCR(I)[IDE(I)] observed for different wavelengths we modified the hot spot model of [9]. We assumed that the resistive state starts in the SNSPD only at the current, at which the vortex becomes unpinned from the hot spot. Using this correction to the model of [9] we were able to explain observed field dependence of PCR(I) at all studied wavelengths for both materials.

II. EXPERIMENT

In our experiments we used a cryoinsert with a superconducting solenoid for the storage dewar in which operation temperature 1.7 K was achieved by helium vapor evacuation. Magnetic fields from 0 to 425 mT were applied perpendicular to the SNSPD plane. The SNSPD was fixed to a sample holder in a dipstick and was wire bonded to a transmission line with a coplanar-coaxial connector. The SNSPD chip with the transmission line was connected to a dc plus rf output port of a bias-T. The dc port was connected with a precision voltage source. Absorption of a photon produces a voltage pulse which is amplified by two room-temperature Mini-Circuits ZFL-1000LN+ (1-GHz band, 46-dB total amplification) amplifiers, and it is fed to a digital oscilloscope and a pulse counter. We recorded the count rate during a 1-s interval at each current. As a light source we used a grating spectrometer with a black body for wavelengths from 400 to 1550 nm. The light is delivered to the SNSPD by an optical fiber SMF-28e with 9-μm mode field diameter. The meanders were precisely aligned against the fiber core and illuminated from the top side.

TABLE I. Material and physical properties (at $T = 1.7$ K) of studied NbN based SNSPD. $I_{\rm dep}$ is the calculated depairing current and $I_c(0)$ is a critical current of the detector at zero magnetic field. Coefficients $\beta_{\rm exp}$ and $\beta_{\rm th}$ are related to the current dependence of the dark count rate (see Sec. IV).

Sample	w (nm)	d (nm)	T_c (K)	$I_c(0)$ (μA)	$R_{\rm sq}$ (Ω)	ξ (nm)	$I_{\rm dep}$ (μA)	$\beta_{\rm exp}$	$\beta_{\rm th}$
NbN1	102	4	10.1	27.1	512	4.9	44	108	208
NbN2	90	6	9.9	21.2	456	4.7	45	85	227
NbN3	110	5	9.2	25.1	420	4.7	57	83	232

We studied three NbN detectors with different material and physical parameters (see the Table I). Only one of the detectors (NbN1) shows well-determined saturation of the photon count rate at large currents in a wide range of wavelengths $\lambda = 450$–1000 nm (see Fig. 1) and we mainly present results for this detector. In Fig. 1 we use a linear scale to demonstrate the clear saturation of PCR and maximal IDE $\simeq 1$. Only for wavelengths $\lambda = 1200$ and 1550 nm intrinsic detection efficiency does not reach unity [for these wavelengths we find PCR$_{\rm sat}$ by extrapolation of the experimental data to larger currents using similarity between shapes of PCR(I) for different wavelengths—see Fig. 1].

In Fig. 2 we show the effect of the external magnetic field H on the photon count rate for photons with different energies (wavelengths). When current approaches the critical current of the meander $I_c(H)$ [its dependence on H is shown in the inset in Fig. 2(d)] the dark counts strongly interfere with photon counts, and we did not show IDE(PCR) in this current range (also as in Fig. 1). The effect of magnetic field is very similar to the one found before in [14] for the MoSi detector—with increase of H dependence PCR(I) shifts to the direction of *small* currents and this shift is smaller the higher the energy of the photon. The new effect which was not observed before is the *decrease* of PCR (when IDE $\gtrsim 0.5$) at currents larger

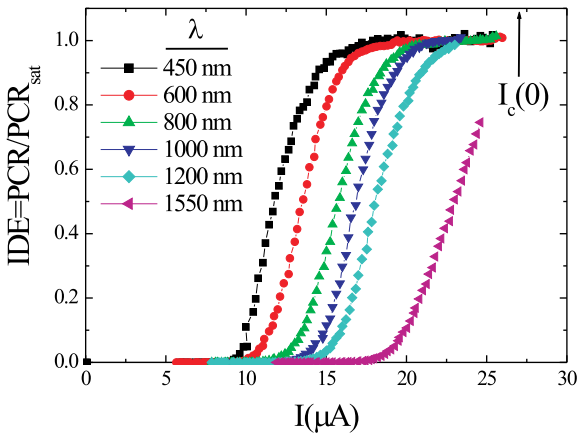

FIG. 1. (Color online) Current dependence of the normalized photon count rate [PCR/PCR$_{\rm sat}$($H = 0$) = IDE] for different wavelengths found for good quality detector NbN1. For λ=1200 and 1550 nm we find PCR$_{\rm sat}$($H = 0$) from extrapolation of the experimental results to larger currents and assuming small variation of the shape of dependence IDE(I) with change of λ.

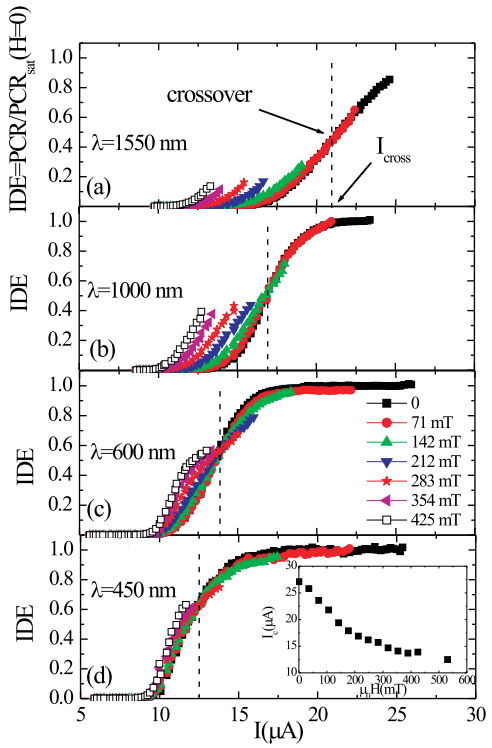

FIG. 2. (Color online) IDE(I) of the NbN1 detector at different magnetic fields. In the inset in panel (d) we present experimental field dependence of the critical current of this detector.

than "crossover" current $I_{\rm cross}$—see Fig. 2. At large magnetic fields the effect is not visible because $I_c(H)$ rapidly decreases and dark counts interfere with the photon counts before IDE reaches $\simeq 0.5$.

We observed the same crossover behavior also for NbN2 and NbN3 detectors for photons with $\lambda = 500$–800 nm when PCR saturated at $H = 0$. For the MoSi detector the crossover was not found and dependence IDE(I) just shifted to the direction of small currents (for this specific detector PCR did not saturate even for photons with $\lambda = 450$ nm).

Dependence of dark count rate (DCR) on the magnetic field for the NbN1 detector is shown in Fig. 3. DCR follows the

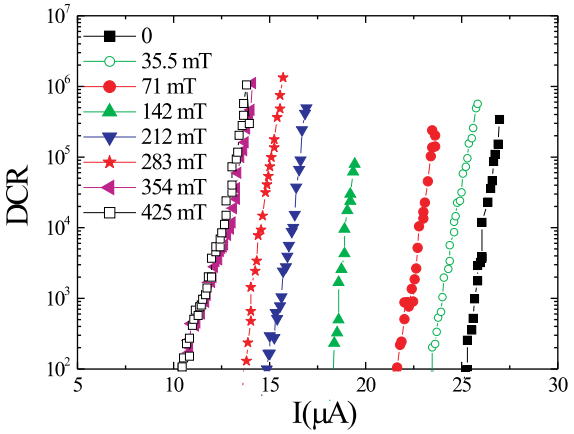

FIG. 3. (Color online) Dark count rate in the NbN1 detector at different magnetic fields.

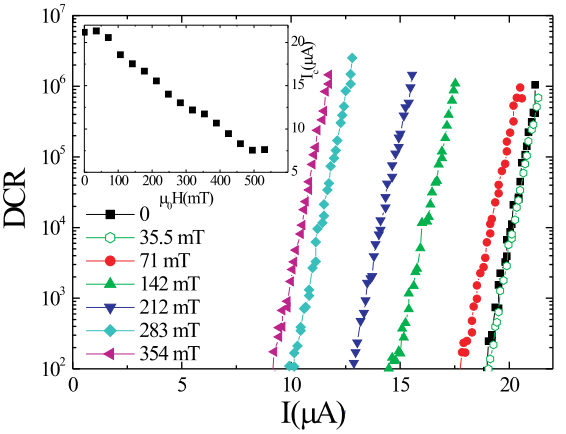

FIG. 4. (Color online) Dark count rate and experimental critical current (in the inset) of the NbN2 detector at different magnetic fields.

change in the critical current of the meander and curve DCR(I) shifts to smaller currents with increasing H (it coincides with the result found in [14] for the MoSi detector). Notice that the shift is well visible even for $\mu_0 H \leqslant 71$ mT, at which photon count rate practically does not change for all studied wavelengths. On the contrary, at large magnetic fields DCR slightly depends on H [because of the small change in the critical current—see inset in Fig. 2(d)], while photon count rate shows noticeable field dependence (at least for photons with $\lambda = 1000$–1500 nm).

In Fig. 4 we show dark count rate and critical current of the NbN2 detector measured at different magnetic fields. At low magnetic fields ($\mu_0 H \leqslant 36$ mT) the critical current practically does not depend on H and DCR does. This result is in drastic contrast with results for the NbN1 detector [see inset in Figs. 2(d) and 3] and theoretically predicted linear decay of the critical current in narrow superconducting strips at low H [13,31]. As we discuss in Sec. III B, a plateau in dependence $I_c(H)$ at $H \to 0$ may appear if there is a relatively large intrinsic defect in the middle of the nanowire and the resistive state starts via nucleation of the vortex-antivortex pair in that place. Detailed discussion of current dependence of DCR for different detectors and its relation with existing theories is postponed for Sec. IV.

III. THEORY

To calculate dependence IDE(I,H) we use the model of [9] (with one important modification which is discussed in Sec. III A). The hot spot (HS) is modeled as a region in the form of a circle with radius R and inside this area the quasiparticle distribution function $f(\epsilon)$ deviates from the equilibrium (the quasiparticles are "heated") [9]. Because of heated quasiparticles the superconducting order parameter $\Delta = |\Delta| e^{i\varphi}$ is suppressed inside the hot spot and the critical current of the nanowire changes. Our aim is to find its value (we call it the detection current $I_{\rm det}$ to distinguish it from the critical current I_c of the nanowire without a hot spot) by solving the Ginzburg-Landau equation for Δ:

$$\xi_{\rm GL}^2 \left(\nabla - \frac{2ieA}{\hbar c}\right)^2 \Delta + \left(1 - \frac{T}{T_c} + \Phi_1 - \frac{|\Delta|^2}{\Delta_{\rm GL}^2}\right)\Delta = 0. \quad (1)$$

The term [15–17]

$$\Phi_1 = \int_{|\Delta|}^{\infty} \frac{2(f^0 - f)}{\sqrt{\epsilon^2 - |\Delta|^2}} d\epsilon \qquad (2)$$

describes the effect of nonequilibrium distribution function $f(\epsilon) \neq f^0(\epsilon) = 1/[\exp(\epsilon/k_BT) + 1]$ on Δ. In Eq. (1) $\xi_{GL}^2 = \pi\hbar D/8k_BT_c$ and $\Delta_{GL}^2 = 8\pi^2(k_BT_c)^2/7\zeta(3) \simeq 9.36(k_BT_c)^2$ are the zero-temperature Ginzburg-Landau coherence length and superconducting order parameter, respectively. For numerical calculations it is convenient to write Eq. (1) in dimensionless units [length is scaled in units of $\xi(T) = \xi_{GL}/(1 - T/T_c)^{1/2}$, Δ is scaled in units of $\Delta_{eq} = \Delta_{GL}(1 - T/T_c)^{1/2}$, and vector potential A is scaled in units of ξH_{c2}, where H_{c2} is the second critical magnetic field]:

$$(\nabla - i\tilde{A})^2\tilde{\Delta} + (\alpha - |\tilde{\Delta}|^2)\tilde{\Delta} = 0, \qquad (3)$$

with $\alpha = (1 - T/T_c + \Phi_1)/(1 - T/T_c)$.

In our model we have two control parameters: the radius of the hot spot and the value of Δ inside the HS (Δ_{in}), which is controlled by the parameter α in Eq. (3) [or Φ_1 in Eq. (1)]. In contrast with other hot spot models (see, for example, [1,3,6–8]) our approach automatically resolves the question about stability of the superconducting state of the nanowire without usage of extra assumptions (like the additional condition for vortex entry needed in the London model) and it takes into account the current continuity equation $\mathrm{div}\, j = 0$ [which comes from the imaginary part of Eq. (1) or Eq. (3)]. The drawback of our approach is the unknown quantitative relation between the energy of the absorbed photon and the size of the hot spot and how strong Δ is suppressed inside it [those characteristics have to be found from the solution of the kinetic equation for $f(\epsilon)$ coupled with the equation for Δ]. Due to that, we cannot give a quantitative description of experimental results. However our theoretical findings explain qualitatively the experimental field dependence of the photon count rate (see results below) and give us the hope that the used model captures the essential physics of the detection mechanism of single photons in a SNSPD.

A. Straight nanowire

In simulations we place the hot spot in different places across the straight nanowire and find dependence $I_{det}(x)$ (where x is a coordinate of the center of the HS) via numerical solution of Eq. (3) (details of the numerical scheme are presented in [9]). When the photon is absorbed at the edge of the nanowire we model the hot spot by a semicircle with a radius $\sqrt{2}$ times larger than the radius of the hot spot inside the nanowire [5,9].

The resistive state is realized via nucleation of the vortices and their motion across the superconductor [9]. A vortex can enter via the edge of the nanowire when the HS is located near the edge or a vortex-antivortex pair nucleates inside the HS when it is located near a center of the nanowire. In [9] it was found that a relatively large hot spot could pin the vortex when it enters the nanowire and one needs to increase the bias current to make it unpinned. Unlike the usual pinning center, the hot spot relaxes in time and at some moment the vortex could be unpinned even if the current is smaller than the depinning current. Based on this idea the detection current in [9] was

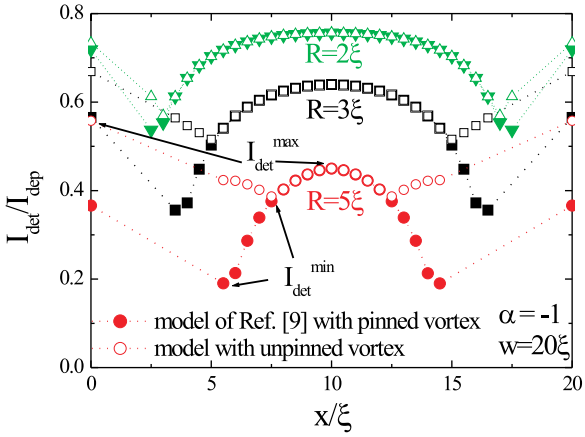

FIG. 5. (Color online) Dependence of the detection current I_{det} (at which the resistive response appears in the SNSPD after photon absorption) on the position of the hot spot across the nanowire, following from the model with a pinned vortex [9] (solid symbols) and the model with an unpinned vortex (empty symbols). The detection current is normalized in units of depairing current I_{dep} and the origin of the x coordinate is at the left edge of the strip. I_{det}^{min} and I_{det}^{max} correspond to the minimal and maximal detection current in two models for HS with $R = 5\xi$.

defined as the current at which the vortex enters the hot spot and it becomes unpinned only when the HS 'dissociates'.

In the present work we define I_{det} as the current at which the vortex overcomes the pinning potential of the hot spot without its "dissociation" (in definitions of [9] $I_{det} = I_{pass}$ for any location of the HS). Figure 5 demonstrates a clear difference in the value of I_{det} following from these two models. The pinning ability of the HS (and the corresponding difference in I_{det}) depends not only on its radius but also on Δ_{in}. For example, when $\alpha = 0$ (it provides larger Δ_{in} than $\alpha = -1$) the hot spot with $R = 2\xi$ already cannot pin vortices (at $H = 0$ and width of the nanowire $w = 20\xi$) and the current at which the vortex enters the hot spot coincides with the current when it becomes unpinned. For $R = 5\xi$ the hot spot cannot pin the vortex anywhere in the nanowire when $\alpha \geqslant 0.36$ (it corresponds to $\Delta_{in} \geqslant 0.6\Delta_{eq}$ inside the HS).

In Fig. 6 we show how I_{det} changes in the magnetic field. In the present model with an unpinned vortex the minimal detection current I_{det}^{min} changes slightly at weak magnetic field ($H < H_s \simeq \Phi_0/2\pi\xi w$, with $H_s \simeq 0.05H_{c2}$ for the nanowire with $w = 20\xi$) when the radius of the hot spot is large and vortex pinning is strong. The physical reason for the found effect is the following—the external magnetic field favors the vortex entry to the HS because of the increase of the current density at the edge of the nanowire [9] but it weakly changes the current density near the nanowire's center, which is important from the point of view of vortex unpinning. When the pinning ability by the HS is weak (as for the hot spot with radius $R = 2\xi$) the change of I_{det}^{min} is large and it practically follows the change of the current density at the edge of the nanowire due to the external magnetic field.

The intrinsic detection efficiency at given current I in our model is determined as a photon-sensitive part of the nanowire where $I > I_{det}(x)$ [9]. In Fig. 7 we present calculated IDE

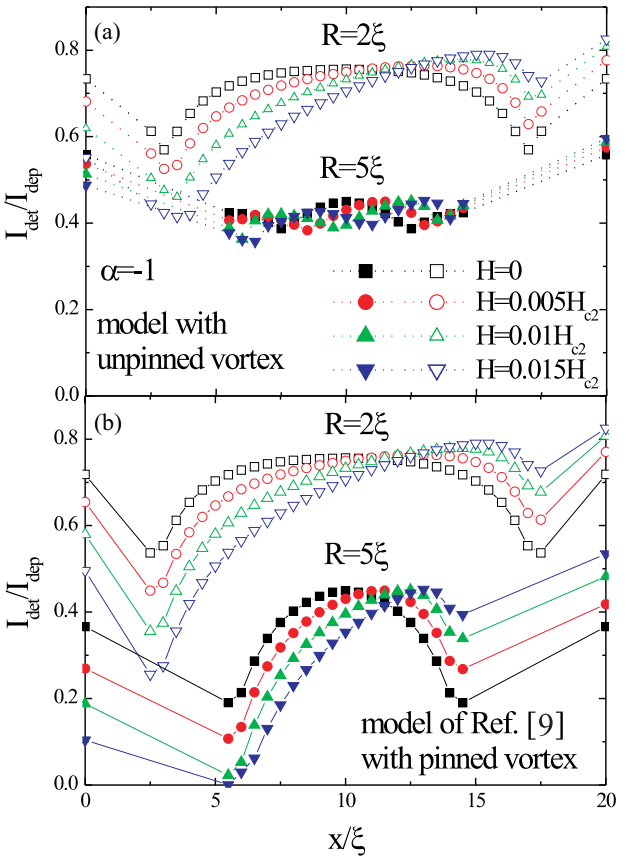

FIG. 6. (Color online) Dependence of the detection current $I_{\rm det}$ on the coordinate of the hot spot (with two radii) at different magnetic fields. Panel (a) corresponds to the model with an unpinned vortex and panel (b) corresponds to the model with a pinned vortex of [9].

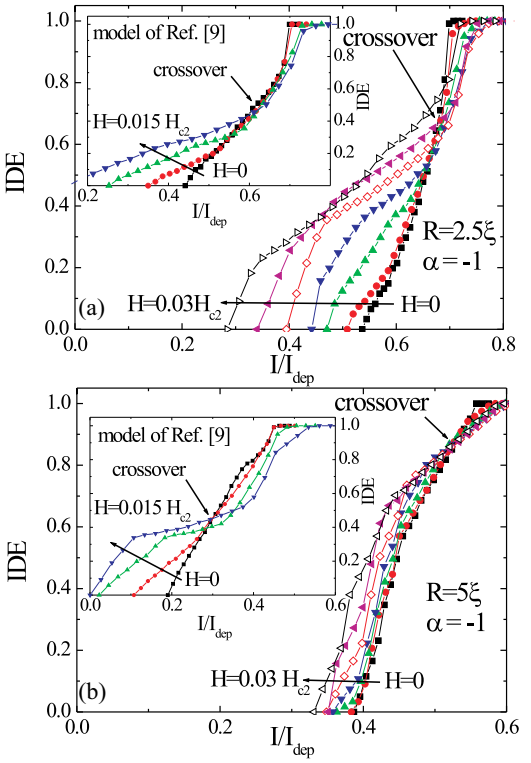

FIG. 7. (Color online) Current dependence of IDE at different magnetic fields (from $H = 0$ to $0.03H_{c2}$ with step $\delta H = 0.005H_{c2}$) following from the vortex hot spot model with an unpinned vortex. Panel (a) corresponds to the hot spot with radius $R = 2.5\xi$ while panel (b) corresponds to the hot spot with $R = 5\xi$ (in both cases $\alpha = -1$). In the insets similar dependencies are present for the hot spot model with a pinned vortex of [9].

at different magnetic fields (magnetic field $0.005H_{c2}$ for the NbN1 detector is equal to 69 mT) and different radii of the hot spot.

First of all, from Fig. 7 one can see that in both models and for all radii of the hot spot there is a crossover current above which IDE *decreases* while at $I < I_{\rm cross}$ IDE *increases* with increase of the magnetic field. The first effect comes from the increase of $I_{\rm det}^{\rm max}$ while the second effect originates from decrease of $I_{\rm det}^{\rm min}$ (see Fig. 6). Second, in the model with the pinned vortex there is strong dependence of IDE on the magnetic field (see insets in Fig. 7) for all radii of the HS while in the model with the unpinned vortex the field dependence is determined by its radius—the larger the radius the weaker field dependence.

In addition we considered hot spots with *fixed* radius $R = 5\xi$ and varying coefficient α in the range 0–0.64, which corresponds to $\Delta_{\rm in} = 0 - 0.8\Delta_{eq}$ (in the absence of transport current and magnetic field). We find that for all values of α there is crossover current and with decreasing α field dependence of IDE(I) becomes weaker (again due to increased ability of the hot spot to pin the vortex).

We studied how the presence of edge defects may influence photon count rate and IDE. First of all, we considered uniform suppression of the critical temperature along the nanowire's edges (in the area with width $\delta x = \xi/2$) where we put $\alpha = -1$. Such a "dead" layer influences quantitatively the shape of dependence IDE(I, H) (compare Figs. 7 and 8). We also calculated IDE(I, H) for another type of the edge defect (pointlike suppression of T_c at the edge) and different values of coefficient α inside the hot spot. All these changes lead

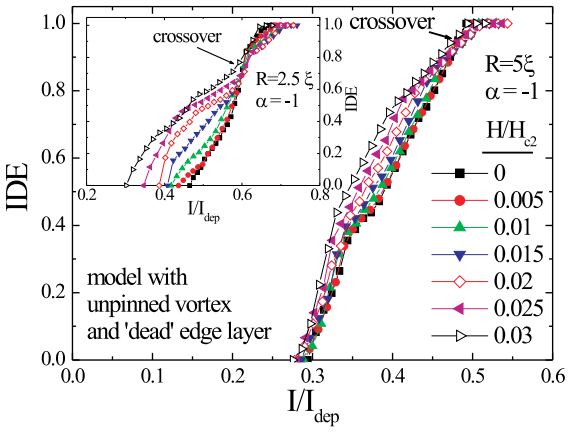

FIG. 8. (Color online) Current dependence of IDE at different magnetic fields following from the vortex hot spot model with an unpinned vortex and "dead" edge layers in the nanowire, where T_c is locally suppressed.

to quantitative variation of IDE(I,H) (not shown here) but qualitative properties [namely, the presence of the crossover current and dependence of IDE(H) on the pinning ability of the hot spot] stayed the same.

B. Effect of meander geometry and bulk intrinsic defects

We have to stress that the results present in Figs. 5–8 correspond to the straight nanowire, while real detectors have the form of the meander. In Fig. 9 we show calculated field dependence of the critical current of the meander with geometrical parameters close to experimental ones (see insets in Fig. 9) and the straight nanowire with width $w = 20\xi$. We choose such a bend of the meander where the magnetic field suppresses the critical current (for the opposite bend or the opposite current direction the same magnetic field enhances I_c [18]). Because of the current crowding effect $I_c(H)$ of the meander is substantially smaller than $I_c(H)$ of the straight nanowire [18] (the difference is not large at zero magnetic field but it is more pronounced at finite H) and it makes unreachable large values of IDE ~ 1 calculated at finite H and shown in Figs. 7 and 8 for the straight nanowire. When the current approaches $I_c(H)$ the dark counts will interfere with the photon counts and the SNSPD stops working.

It is interesting to note that there are no vortices in the narrow part of the meander at $I \lesssim I_c(H)$ up to the field $H = 0.038H_{c2}$. On the contrary, vortices enter the wide region at field $H \geqslant 0.013H_{c2}$. It occurs due to the smaller value of the critical magnetic field $H_s \simeq \Phi_0/\xi w$ at which vortices may enter the superconducting nanowire [13].

From Fig. 6 one can see that when the hot spot is located close to the center of the straight nanowire $I_{\rm det}$ changes much more weakly with the field increase in comparison with $I_{\rm det}$ for the hot spot placed near or at the edge. From the physical point of view the effect of the hot spot is similar to the effect of the intrinsic defect (where locally either T_c is suppressed or the nanowire is thinner) on I_c. Therefore, the reason for plateaulike $I_c(H)$ dependence found for the NbN2 detector at low magnetic fields (see the inset of Fig. 4) could be a relatively large intrinsic defect which is located somewhere in the middle of straight pieces of the meander. We have to stress here that such a "plateau" may exist if there is no intrinsic defect in the nanowire (see empty squares in Fig. 9, for example). It appears when $I_c(0) \simeq I_{\rm dep}$ [19,20] due to the depairing effect of the superconducting current (supervelocity). But in our detectors $I_c(0)$ is far below $I_{\rm dep}$ (see Table I) and this effect could be skipped.

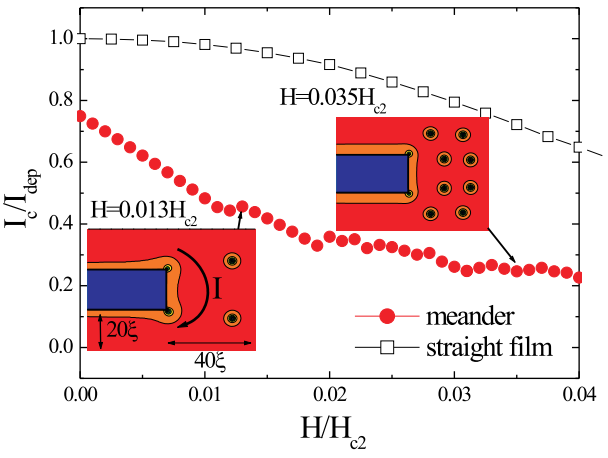

FIG. 9. (Color online) Numerically calculated magnetic field dependence of the critical current I_c of the straight nanowire with $w = 20\xi$ (empty squares) and the meander (solid circles) with geometrical parameters shown on the bottom inset. For the meander we take into account the bend where the external magnetic field decreases the critical current. In the insets we show the contour plot of $|\Delta|$ for the meander at different magnetic fields and $I \lesssim I_c(H)$. At $H \leqslant 0.012H_{c2}$ there are no vortices in the meander. In the narrowest place of the meander vortices appear at $H > 0.038H_{c2}$.

Intrinsic defects may influence I_c not only at low magnetic fields but also at relatively large fields, when vortices exist in the meander at $I \lesssim I_c(H)$. Indeed, calculated $I_c(H)$ decays faster than the experimental one [compare Fig. 9 with the inset in Fig. 2(d)] at the magnetic field $H \gtrsim 0.015H_{c2}$ ($\mu_0 H \gtrsim$ 207 mT for the NbN1 sample) when I_c changes nonlinearly with H. Such a deviation could be explained by the vortex pinning at the intrinsic defects of the nanowire which are absent in our calculations. A similar effect was observed for NbN straight strips in the recent experiment [21] and analytically it was calculated in [22] for the bulk pinning described by the Bean model. Vortex pinning should prevent fast decay of $I_{\rm det}^{\rm min}$ with increase of H (in this case the vortex has to overcome not only the pinning from the hot spot but also the intrinsic pinning outside the HS) and it has to be taken into account for quantitative comparison of experimental and theoretical IDE(I) at magnetic fields larger than $0.015H_{c2}$.

Now we would like to discuss contribution of the bends to detection ability of the meanderlike detectors. Because of the current crowding effect the region near the interior corner of the bend is capable of detecting photons at the currents lower than the minimal detection current $I_{\rm det}^{\rm min}$ of the straight nanowire. Rough estimation, based on the difference between the critical current of the meander and the straight nanowire, indicates that the near-corner area stops to detect photons at the current $I^{\rm min} = I_{\rm det}^{\rm min} \times I_c^{\rm meander}/I_c^{\rm nanowire}$.

Using numerical simulations we find area S near the bend where the local current density is larger (we use criteria $j > 1.01\,j_\infty$) than the current density far from the bend j_∞. For our geometrical parameters (see insets in Fig. 9) we find $S \simeq 400\xi^2 \sim w^2$. For parameters of the NbN1 meander this near-bends area comprises about 1.4% of the whole area of the detector and it gives us the rough estimation for the photon-sensitive area at the currents just below $I_{\rm det}^{\rm min}$. When the current decreases further this area shrinks as $I \to I^{\rm min}$. Therefore we suggest that finite $0 <$ IDE $\lesssim 0.014$ in the current range $I^{\rm min} < I < I_{\rm det}^{\rm min}$ comes from this photon-sensitive area located near the interior corners of the meander. This suggestion is also supported by very weak-field dependence of IDE(H) $\ll 1$ observed in our experiment at $\mu_0 H < 70$ mT. If finite and small IDE would be connected with thermoactivated vortex entry (as it was assumed in [6,9]) it should have strong-field dependence in the same range of magnetic fields as the dark count rate has (see Figs. 3 and 4). But if our idea is correct, then IDE should not change (or change very slightly) because of the presence of the *right* and *left* bends in the meander. Indeed, the external magnetic field increases the current density in

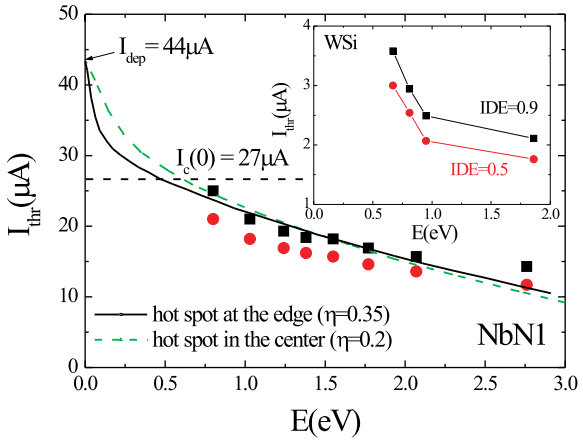

FIG. 10. (Color online) Dependence of the current, at which experimental IDE reaches 0.9 (squares) and 0.5 (circles), on the energy of the photon (results are obtained for the NbN1 detector). The theoretical curves (solid and dashed) are found in assumption that current $I_{\rm thr}$ is equal to the detection current for the hot spot located in the center of the nanowire or at its edge (in the last case it has the form of a semicircle). Fitting coefficient η describes what part of the photon's energy goes for suppression of Δ inside the hot spot [23]. In the inset we show results for the WSi based detector extracted from Fig. 2 of [24].

one kind of bend (let it be the right one for definiteness) and decreases it in another one. We calculate the change in the area near both bends where current density is locally enhanced and find that this area practically does not vary at low magnetic fields because its expansion near the right bend is compensated by its shrinkage near the left bend.

C. Threshold current versus photon energy

In Fig. 10 we show experimental dependence of the current (we call it threshold current $I_{\rm thr}$), at which IDE reaches 0.9, on the energy of the photon E. Our choice of the cutoff is not accidental. Indeed, in the bend region there is a large area where the current density is smaller than j_∞ and this part participates in photon detection at larger currents than the straight pieces of the meander. Roughly, for our geometrical parameters this area is about 10% of the area of the meander. Hence, when the current approaches $I_{\rm det}^{\rm max}$ of the straight nanowire the intrinsic detection efficiency of the meander reaches 0.9 and to reach IDE = 1 one should increase the current further.

In Fig. 10 we also plot theoretical dependencies, following from the vortex hot spot model developed here. We use two locations of the hot spot (in the center and at the edge of the nanowire) and fitting parameter η, which describes what part of the energy of the photon goes for suppression of Δ inside the hot spot [23]. Our model predicts nonlinear dependence $I_{\rm thr}(E)$ (which qualitatively resembles experimental results—see Fig. 10) and rapid growth of $I_{\rm thr}$ up to $I_{\rm dep}$ as $E \to 0$ (unfortunately there are no experimental results in this energy interval). The quantitative agreement between the theory and the experiment is poor, which justifies that the used model assumptions are too rough. Indeed, the shape of the hot spot is not obligatorily round, because in the presence of the transport current the HS will preferably grow in the direction perpendicular to the current flow (due to the current crowding effect). Also the coefficient η may depend on the energy of the photon. Both these factors are not considered in our model, because they need calculation of the dynamics of nonequilibrium quasiparticles and solution of the kinetic equation.

Our experimental dependence $I_{\rm thr}(E)$ drastically differs from the linear relation found in [25] for a superconducting NbN bridge. Note that very similar nonlinear dependence follows from the measurements on a WSi based detector (see inset in Fig. 10— the data were extracted from Fig. 2 of [24]). We checked that for other cutoffs (we take IDE = 0.5 and 0.01) the dependence $I_{\rm thr}(E)$ is still nonlinear (in Fig. 10 we show results for cutoff IDE = 0.5). The reason for the difference with [25] is not clear to us.

IV. DISCUSSION

Our experimental results correlate with preceding experiments where the effect of magnetic field on photon and dark count rate in the SNSPD was studied. In [26,27] no effect of low magnetic field on PCR was observed (for TaN and NbN based detectors, respectively) while in the same range of magnetic fields the dark count rate demonstrated strong-field dependence. The absence of change of PCR in [26] is probably connected with the low value of the maximal magnetic field used in the experiment ($\mu_0 H_{\rm max} = 10$ mT). In [27] authors observed an increase of PCR at larger magnetic fields and found that the value of the effect depends on the wavelength—the smaller λ the smaller the change of PCR (a similar result was found in [14] for the MoSi detector). A small *decrease* of PCR was observed in [27] (see the bump at low magnetic fields and $I = 0.78 I_{c,e}$ in Fig. 3 of [27]) but this effect was not discussed in that paper.

In recent work [28] photon count rate in a superconducting NbN bridge (with width $w = 150$ nm) was measured at different magnetic fields and the authors found field dependence of PCR at $\mu_0 H \gtrsim 30$ mT. From presented results in Fig. 4 of [28] on experimental dependence $I_c(H)$, we may conclude that somewhere in the middle of the bridge the intrinsic defect exists and it leads to weak variation of I_c at $\mu_0 H \lesssim 30$ mT (like in our NbN2 detector—see inset in our Fig. 4). This "weak" place most probably provides a finite count rate at low currents (when IDE $\ll 1$) and PCR rapidly grows with the current increase due to expansion of the photon-sensitive area near that place (like near a bend in the meander). At $\mu_0 H \gtrsim 30$ mT experimental I_c starts to decay with increase of magnetic field, which means that at these fields the "weakest" place is located at the edge of the bridge (due to large edge screening currents produced by an applied magnetic field). It is accompanied by field dependence of the photon count rate, qualitatively similar to our experimental findings for large wavelengths. Unfortunately in [28] only one wavelength ($\lambda = 826$ nm) was used and we cannot be sure in our treatment of their results. Because in [28] PCR did not saturate at large currents the crossover current could not be observed.

In [14,27] the authors compared experimental PCR(H) with prediction of the hot belt model [6] and found large quantitative disagreement. We believe that the hot belt model of [6] is not

able to explain the decrease of PCR (when PCR $\simeq$ PCR$_{sat}$ and IDE $\simeq 1$) at weak magnetic fields and stronger-field dependence of PCR for photons of smaller energies (see our arguments in the Introduction). These properties appear as inevitable consequences of our vortex hot spot model and they are robust with respect to the presence of edge or bulk defects which affect them only quantitatively [they may change the position of the crossover current and influence quantitatively the dependence of PCR(H) at relatively large magnetic fields].

Due to very weak-field dependence of the photon count rate at low magnetic fields $\mu_0 H \lesssim 70$ mT for all studied wavelengths ($\lambda = 450$–1550 nm) we conclude that fluctuation-activated vortex entry to the hot spot plays no role in the photon counting for our NbN detectors. On the contrary, the dark counts are most probably connected with fluctuation assisted vortex nucleation in the nanowire near the "weakest" place (intrinsic defect). It is justified from the shift of DCR(I) in the magnetic field which follows the change in the critical current of the superconducting meander [see Fig. 2(d), inset, and Figs. 3 and 4] and from fast decay of DCR $\sim \exp(-\delta F/k_B T)$ with current decrease, which is a consequence of the current dependent energy barrier for vortex entry $\delta F(I)$ [29–32]. For all studied detectors the logarithm of the dark count rate could be fitted by the linear function $\ln(\mathrm{DCR}) = -\beta_{exp}[1 - I/I_c(H)]$, where the coefficient β_{exp}, extracted from fitting of experimental data at $H = 0$, is shown in Table I.

Using the widely used expression for $\delta F(I)$ following from the London model [31] and its expansion near the critical current, $\delta F \simeq (1 - I/I_c)\Phi_0^2 d/16\pi^2\lambda_L^2$ [see Eq. (2) in [32], where λ_L is the London penetration depth], we calculated $\beta_{th} = \Phi_0^2 d/16\pi^2\lambda_L^2 k_B T$ for each detector (see Table I). The large quantitative difference between β_{exp} and β_{th} we explain by the effect of intrinsic edge or bulk defects and bends in the meander, the role of which was not taken into account in [31]. Indeed, in [32] it was shown that δF is determined by the geometric parameters of the bend and it could be much smaller than in the straight strip at $I/I_c \simeq 1$. We expect the same influence on δF by geometric edge defects (notches), which affect the current distribution in the strip and provide current crowding similar to the effect of the bend.

We have to stress that the intrinsic defect could be located not only at the edges but also in the middle of straight pieces of the meander. The field dependence of I_c is individually characteristic of the detector [compare insets in Figs. 2(d) and 4] because it is determined by position and size of the largest intrinsic defect. In general $I_c(H)$ may not be a linear function of H at low magnetic fields, as it was predicted in several works—see, for example, [6,13]. Because the energy barrier for vortex entry (or nucleation of the vortex-antivortex pair) goes to zero at $I = I_c$ and it is the smallest one near the largest intrinsic defect, the field dependence of the dark count rate is also individually characteristic of the detector (compare Figs. 3 and 4) and depends not only on the thickness, width of the nanowire, and λ_L but also on the parameters of the defect.

V. CONCLUSION

The experiment on the magnetic field dependence of photon count rate in the NbN based SNSPD revealed the following three main features.

(1) At low magnetic fields ($\mu_0 H \lesssim 70$ mT) PCR very weakly depends on magnetic field (for studied wavelengths $\lambda = 450$–1550 nm), while dark count rate has pronounced field dependence.

(2) At larger fields PCR changes with magnetic field and the smaller the energy of the photon the stronger the field dependence of PCR.

(3) For all studied wavelengths there is a crossover current above which PCR slightly *decreases* while at $I < I_{cross}$ PCR *increases* with increasing magnetic field. Crossover current is located close to the current at which PCR(I) saturates and reaches a plateau.

All observed features could be explained by the present vortex hot spot model. Its main properties are the following.

(i) In the vortex hot spot model it is assumed that the absorbed photon creates the finite region with partially suppressed Δ (hot spot)—like in any hot spot model. Appearance of such a region changes the critical current of the nanowire. The resistive state starts at some detection current I_{det} via nucleation of the vortex-antivortex pair inside the HS and their motion across the nanowire if HS is located close to the center of the superconductor (the same as in [9]). If the hot spot is located close to the edge of the nanowire the resistive state is realized via single vortex entrance via the edge and its free motion across the hot spot and nanowire (without "dissociation" of the hot spot, as it was needed in [9]).

(ii) Detection current depends nonmonotonically on the position of the hot spot across the nanowire and has maximal I_{det}^{max} and minimal I_{det}^{min} values. Photon count rate reaches a maximum when applied current becomes larger than I_{det}^{max} and PCR gradually decreases with decreasing current due to shrinkage of the photon-sensitive area. This property is qualitatively the same as in the model of [9].

(iii) Perpendicular magnetic field induces the screening currents in the nanowire, which makes current distribution nonuniform across the superconductor. It leads to decreasing of I_{det}^{min} and increasing of I_{det}^{max}, which explains the existence of the crossover current in the experiment. This property is qualitatively the same as in the model of [9] and qualitatively coincides with experimental finding (3).

(iv) When the" hot spot is large (in units of coherence length) and Δ is strongly suppressed inside the HS it can pin vortices and both I_{det}^{min} and I_{det}^{max} slightly vary at relatively low magnetic fields $H \lesssim H_s$. The hot spots with small size and/or slightly suppressed Δ produce weak pinning, and the detection current changes in the same magnetic field much more strongly. It explains property (2) found in the experiment and discriminates the present model from the model of [9].

(v) In the detectors made in the form of a meander there are right and left bends. At small currents and weak magnetic fields the regions near the bends are responsible for the finite photon count rate due to locally enhanced current density. With increasing magnetic field the area where the current density is locally enhanced in right and left bends practically does not change because in one kind of bends current density decreases while in another it increases. The increase of photon count rate starts only when $I_{det}^{min}(H)$ of the straight part of the meander approaches the transport current.

ACKNOWLEDGMENTS

The work was partially supported by the Russian Foundation for Basic Research (Project No. 15-42-02365/15). The following authors acknowledge support from the Ministry of Education and Science of the Russian Federation: D.Yu.V. (State Contract No 02.B.49.21.0003), Yu.K. (Unique Identifier of the Scientific Research No. RFMEFI58614x0007), A.K. (State Contract No. 14.B25.31.0007), A.S. (State Task No. 2327), and G.G. (State Task No. 960). A.S. also acknowledges support by a grant of the President of the Russian Federation (Contract No. MK-6184.2014.2), and G.G. acknowledges support by a grant of the President of the Russian Federation (Contract No. NSh-1918.2014.2).We thank SCONTEL company for the SSPD detector and cryoinsert for storage dewar.

[1] A. D. Semenov, G. N. Gol'tsman, and A. A. Korneev, Phys. C (Amsterdam) **351**, 349 (2001).
[2] G. Gol'tsman, O. Okunev, G. Chulkova, A. Lipatov, A. Semenov, K. Smirnov, B. Voronov, A. Dzardanov, C. Williams, and R. Sobolewski, Appl. Phys. Lett. **79**, 705 (2001).
[3] A. Semenov, A. Engel, H.-W. Hübers, K. Il'in, and M. Siegel, Eur. Phys. J. B **47**, 495 (2005).
[4] L. Maingault, M. Tarkhov, I. Florya, A. Semenov, R. Espiau de Lamaëstre, P. Cavalier, G. Gol'tsman, J.-P. Poizat, and J.-C. Villégier, J. Appl. Phys. **107**, 116103 (2010).
[5] A. N. Zotova and D. Y. Vodolazov, Phys. Rev. B **85**, 024509 (2012).
[6] L. N. Bulaevskii, M. J. Graf, and V. G. Kogan, Phys. Rev. B **85**, 014505 (2012).
[7] A. Eftekharian, H. Atikian, and A. H. Majedi, Opt. Express **21**, 3043 (2013).
[8] A. Engel and A. Schilling, J. Appl. Phys. **114**, 214501 (2013).
[9] A. Zotova and D. Y. Vodolazov, Supercond. Sci. Technol. **27**, 125001 (2014).
[10] C. M. Natarajan, M. G. Tanner, and R. H. Hadfield, Supercond. Sci. Technol. **25**, 063001 (2012).
[11] A. Rothwarf and B. N. Taylor, Phys. Rev. Lett. **19**, 27 (1967).
[12] M. Tinkham, *Introduction to Superconductivity* (McGraw-Hill, New York, 1996).
[13] G. Stejic, A. Gurevich, E. Kadyrov, D. Christen, R. Joynt, and D. C. Larbalestier, Phys. Rev. B **49**, 1274 (1994).
[14] A. A. Korneev, Y. P. Korneeva, M. Y. Mikhailov, Y. P. Pershin, A. V. Semenov, D. Y. Vodolazov, A. V. Divochiy, Y. B. Vakhtomin, K. V. Smirnov, A. G. Sivakov, A. Y. Devizenko, and G. N. Goltsman, IEEE Trans. Applied Superconductivity **25**, 2200504 (2015).
[15] B. I. Ivlev, S. G. Lisitsyn, and G. M. Eliashberg, J. Low Temp. Phys. **10**, 449 (1973).
[16] A. I. Larkin and Yu. N. Ovchinnikov, Sov. Phys. JETP **41**, 960 (1975).
[17] L. Kramer and R. J. Watts-Tobin, Phys. Rev. Lett. **40**, 1041 (1978).
[18] J. R. Clem, Y. Mawatari, G. R. Berdiyorov, and F. M. Peeters, Phys. Rev. B **85**, 144511 (2012).
[19] G. M. Maksimova, N. V. Zhelezina, and I. L. Maksimov, Europhys. Lett. **53**, 639 (2001).
[20] V. P. Andratskii, L. M. Grundel', V. N. Gubankov, and N. B. Pavlov, Zh. Eksp. Teor. Fiz. **65**, 1591 (1973) [Sov. Phys. JETP **38**, 794 (1974)].
[21] K. Ilin, D. Henrich, Y. Luck, Y. Liang, M. Siegel, and D. Yu. Vodolazov, Phys. Rev. B **89**, 184511 (2014).
[22] A. A. Elistratov, D. Y. Vodolazov, I. L. Maksimov, and J. R. Clem, Phys. Rev. B **66**, 220506 (2002).
[23] D. Yu. Vodolazov, Phys. Rev. B **90**, 054515 (2014).
[24] B. Baek, A. E. Lita, V. Verma, and S. W. Nam, Appl. Phys. Lett. **98**, 251105 (2011).
[25] J. J. Renema, R. Gaudio, Q. Wang, Z. Zhou, A. Gaggero, F. Mattioli, R. Leoni, D. Sahin, M. J. A. de Dood, A. Fiore, and M. P. van Exter, Phys. Rev. Lett. **112**, 117604 (2014).
[26] A. Engel, A. Schilling, K. Il'in, and M. Siegel, Phys. Rev. B **86**, 140506(R) (2012).
[27] R. Lusche, A. Semenov, Y. Korneeva, A. Trifonov, A. Korneev, G. Gol'tsman, and H.-W. Hübers, Phys. Rev. B **89**, 104513 (2014).
[28] J. J. Renema, R. J. Rengelink, I. Komen, Q. Wang, R. Gaudio, K. P. M. op't Hoog, Z. Zhou, D. Sahin, A. Fiore, P. Kes, J. Aarts, M. P. van Exter, M. J. A. de Dood, and E. F. C. Driessen, Appl. Phys. Lett. **106**, 092602 (2015).
[29] C. Qiu and T. Qian, Phys. Rev. B **77**, 174517 (2008).
[30] H. Bartolf, A. Engel, A. Schilling, K. Il'in, M. Siegel, H.-W. Hubers, and A. Semenov, Phys. Rev. B **81**, 024502 (2010).
[31] L. N. Bulaevskii, M. J. Graf, C. D. Batista, and V. G. Kogan, Phys. Rev. B **83**, 144526 (2011).
[32] D. Y. Vodolazov, Phys. Rev. B **85**, 174507 (2012).